R-823

RECENT DEVELOPMENTS IN PLASMA SPRAYED THERMAL BARRIER COATINGS

Drs. P. FAUCHAIS, A. VARDELLE and M. VARDELLE

L.M.C.T.S. - Equipe Plasma, Laser, Matériaux
Université de Limoges - UPRES A 6015 - Faculté des Sciences
123, Avenue Albert Thomas - 87060 LIMOGES Cedex - FRANCE

Abstract

This paper presents a review of our present knowledge in the formation of plasma sprayed Thermal Barrier Coatings (TBCs). The following points are examined for TBCs made of zirconia partially stabilized with 8 wt % of yttria :

- characteristic times for particle flattening, splat cooling and solidification with the corresponding cooling rates and microstructure.
- critical preheating temperature of substrates or previously deposited layers to achieve a good contact with splats. An explanation of the effect of this critical temperature is proposed.
- times between two impact events at the same location and two successive passes. The consequences on the mean temperature within coating in conjunction are underlined for various substrate and coating cooling devices.
- the effect of substrate critical temperature and substrate oxidation stage on coating adhesion/ cohesion.
- splat layering and temperature conditions at which a columnar structure can grow through the whole coating. The consequences on stresses development during and after spraying and coating Young's modulus, are discussed.
- at last, the parameters which have to be controlled during spraying to achieve a much better reproducibility of coatings. A special emphasize is given to torch voltage fluctuations related to electrodes erosion, powder injection conditions and finally substrate and coating temperature before (preheating) during and after (cooling) spraying.

1. INTRODUCTION

Thermal barrier coatings (TBCs) are now included as part of the initial engine of turbine-powered aircrafts. They make them possible to achieve an average reduction in the metal temperature for turbine blades of 50 to 80°C and reduction of blade hot-spot temperature of up to 139°C. The latter are only a fraction of the capability of TBCs, estimated at 170°C or more [1]. TBCs have also been used in land-based turbine combustors for 10 years, and in diesel engines where graded coatings are highly effective. In all cases, the purpose is to enhance component durability while running the engine operating temperature. In this paper TBCs for diesel engines will not be considered. The difference between nominal requirements for aircraft and power generation turbine applications are summarized in table 1 [2].

Requirement	Commercial aircraft	Power generation
Number of cycles	8000	2,400
Total hours	8000	24,000
Hours at peak conditions	300	24,000
Peak surface temperature	>1204°C (2200°F)	<1204°C (2200°F)
Peak bond coat temperature	1093°C (2000°F)	954°C (1750°F)
Relative size	1x	5x

Table 1 : Comparison of nominal TBC requirements for aircraft and power generation turbine applications [2].

Paper presented at an AGARD SMP Meeting on "Thermal Barrier Coatings", held in Aalborg, Denmark, 15-16 October 1997, and published in R-823.

The main criteria for power generation use of TBCs are the time and temperature effects on bond coat and substrate, coating densification and changes in thermal or mechanical properties of the coatings.

As underlined in reference [3] for advanced land-based gas turbines, the goals that are to be achieved together with issues and challenges are summarized in fig. 1.

For a long period (more than 20 years) TBCs were essentially plasma-sprayed in air (APS) [4-7] or controlled atmosphere [8]. Since a few years Physical Vapor Deposition assisted by Electron Beam (EB-PVD) TBCs, have been available on the market [9,10] especially for aircraft engines. The advantages claimed relatively to APS TBCs are the following :

- a columnar structure under certain conditions of evaporation,
- a fast tapering at the opening of cooling holes while plasma sprayed coatings have a greater tendency to built up coating at that location,
- possibility to achieve much more smoother surfaces,
- high adhesion/cohesion values (~ 70 MPa),
- low residual stress at room temperature (~ 70 MPa),
- reduction of temperature of 38-66°C in stage of High Pressure Turbine Blade,
- high number of cycles in engine testing : 180 for blades and 20000 for engine nozzle.

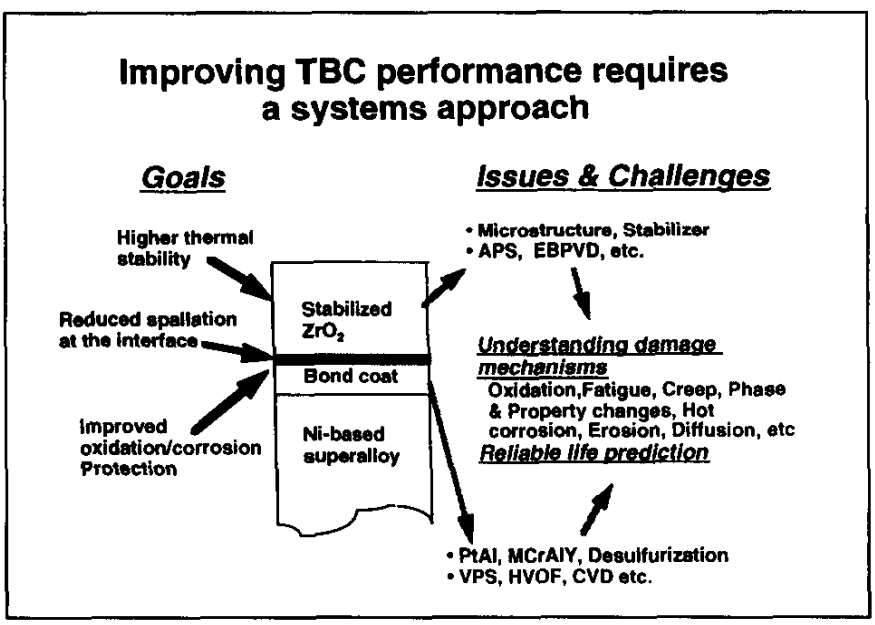

Fig. 1 : Approach for improving TBC performances [3].

However, it does not mean necessarily that APS TBCs have no future. For example they have a significant advantage in being able to accommodate the large size components found in modern large power generation machines. Each component application of a TBC requires careful study and review to determine whether APS or EB-PVD has to be used [3]. Moreover, a better understanding of the APS coating formation could result in coatings with similar properties as those obtained by EB-PVD. The aim of this paper is first to review what is our knowledge in plasma sprayed coating formation. We will first were discuss the splat formation, their layering and the resulting coating adhesion/cohesion as well as residual stresses. We will second underline which parameters have to be controlled during spraying to achieve a much better reproducibility of the plasma spray process.

2. PLASMA SPRAYED COATING FORMATION

All the results presented in this paper concerned fused and crushed powders with 8 wt% Y_2O_3. They are called in the following YSZ.

2.1. Characteristic times and cooling rates

Table 2 summarizes characteristic time values for particles in the size range 22-70 μm sprayed with d.c. torches and impacting at velocities between 80 and 260 m/s on smooth surfaces (Ra < 0.1 μm) [11-14].

Flattening time t_f (μs)	Starting of nucleation t_n (μs)	Solidification time t_s (μs)	Time between two impact events at the same location t_j (μs)	Time between two successive passes t_t (μs)
1-3	0.3-2.5	< 10	500-5000	10^6-10^7

Table 2 : Characteristic times in d.c. plasma spraying.

These various times show clearly that the impacting particles and resulting splats will experience very different temperature histories :

2.1.1. Single splat

Many theoretical studies have been devoted to the impact and flattening of the particles on the substrate (see their description in [14]). All of them, except one, concern impacts on smooth surfaces.

a) Smooth surfaces

Phenomena at impact can be characterized by the particle Weber's number ($We = \rho_p \cdot d \cdot v_p^2/\sigma_p$ where ρ_p, v_p, d are the particle specific mass, impact velocity and diameter respectively and σ_p its surface tension), and Reynolds' number ($Re = \rho_p \cdot v_p \cdot d/\mu_p$ where μ_p is the particle viscosity at impact). When flattening starts, We can be rather high (up to 10000) and the flattening process is independent of particle surface tension which has importance only when flattening is almost completed. These theories end up in relationships giving the particle flattening degree ξ and flattening time t_f as functions of the Reynolds number. ξ is defined as the ratio of the splat diameter D (assumed to have a disk shape) to that of the impacting particle d.

$$\xi = \kappa \cdot R_e^{\alpha} \qquad (1)$$

$$t_f = 2 \cdot d_p \cdot R_e^{0.2}/(3 \cdot v_p) \qquad (2)$$

κ varies between 0.8 and 1.2941 while α is either 0.2 or 0.125 or 0.167.

Typical values for a zirconia particle 30-μm in diameter, impacting at v_p = 200 m/s at a temperature $T_p = T_m \times 1.3$, where T_m is zirconia melting temperature, are for example ξ = 4.8 which corresponds to a splat thickness e_s ~ 1.1 μm and t_f ~ 1 μs. If the impacting particle velocity increases, ξ increases while t_f and e_s decrease and it is the reverse if v_p decreases. The most recent theories have shown that solidification can start before flattening is completed [15]. Solidification depends mainly on [14,15] the wettability of the molten material, the thermal contact resistance R_{th} with the substrate, the splat thickness e_s and the thermal properties of the substrate material. The interfacial contact resistance characterizes the real contact with the substrate or the previously deposited layers. It can vary between 10^{-6} and 10^{-8} m².K/W, the last value corresponding to a perfect contact. Fig. 2 represents the time-temperature evolution of a zirconia splat 1-μm thick for two values of R_{th}. For values below 10^{-7} m².K/W (see fig. 2.a), the temperature T_b of the lower surface of the splat decreases very fast while the substrate surface temperature T_i increases very fast. Over R_{th} = 10^{-7} m².K/W, there is nearly no temperature gradient within the splat (see fig. 2.b) while T_i is much lower.

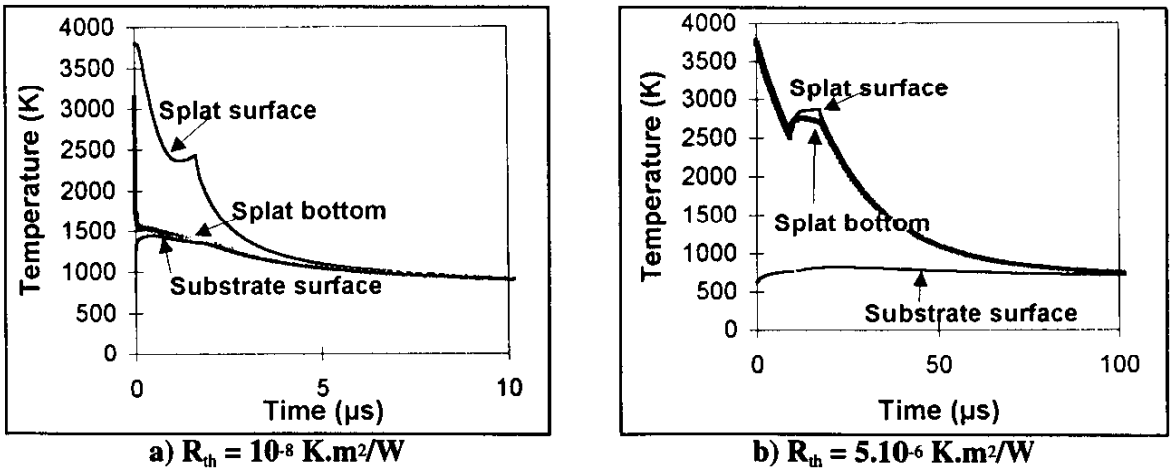

a) $R_{th} = 10^{-8}$ K.m²/W **b) $R_{th} = 5.10^{-6}$ K.m²/W**

Fig. 2 : Splat surface and bottom as well as interface temperature evolutions for two values of R_{th} (1-μm thick Zirconia splat on a smooth stainless steel substrate at 600 K).

In both cases the increase in splat surface temperature is due to the recalescence phenomenon. However, these results, which have been obtained by assuming a constant nucleation temperature of 2500 K and an instantaneous full contact of the whole splat, can be deeply modified if nucleation process is included in the model and the evolution of the contact surface during flattening is accounted for.

The corresponding cooling rates during the first μs are between 10^6 and 10^9 K/s. For $R_{th} < 10^{-7}$ m^2.K/W the heat transfer rate from droplet to substrate is very high and the liquid can be cooled well below the melting point in one microsecond or less. It is therefore quite plausible that in this very short time interval, the liquid does become undercooled and nucleation of crystals is delayed until after the droplet has almost completely spread out.

As shown in fig. 2, if during flattening and just after, the cooling rate is very high, its slows down drastically for times longer than 10 to 50 μs. The splat temperature tends then slowly to the mean substrate and previously deposited layer temperature T_d imposed by torch heating, previously deposited pass thickness and cooling devices.

b) Rough surfaces

Only one model accounting for the substrate roughness has been proposed [16] up to now. The roughness was schemed by cones. This model gives for the flattening degree a relationship similar to (1) but multiplied by a function depending on the cone height and the valley volume. It results, of course, in thicker splats which shape is not that of a disk. Assuming the same value of R_{th} than for smooth substrates, the cooling rate will be lower due to the higher value of e_s.

2.1.2. Layering splats

As powder loading is rather low in plasma spraying [14], statistically a new particle impacts on a previously deposited splat in times t_i of the order of 500-5000 μs i.e. on already solidified splats. The surface temperature of the first splat due to the impact of successive layering splats will depend strongly on R_{th} and the mean temperature of substrate and coating T_d. This leads, as schemed in fig. 3, in impulse reheatings with the first splat surface peak temperature decreasing progressively due to the insulation by the successively deposited splats.

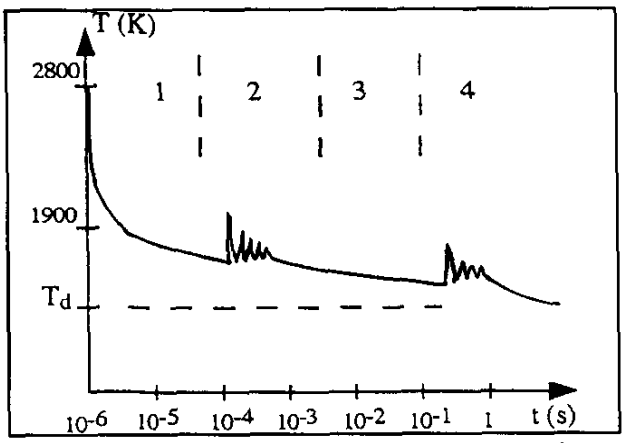

Fig. 3 : Impulse reheating of the first splat surface by the layering splats.

The temperature T_d is linked to :

- substrate preheating temperature T_{ph} ;
- substrate dimension, thickness and thermal properties (controlling the heat sink) ;
- relative movement torch to substrate. This movement determines the pass thickness e_p (the heat content of layered splats increases with e_p which can vary from a few layered splats to a few hundreds) and the time t_t for the torch to come back at the same location (heating by plasma plume flux) ;
- cooling devices used : air jets blowing at the substrate and coating surface, and air barrier blowing orthogonally to the plasma jet to reduce in a ratio up to six the plasma plume heat flux [18], but also cooling down the droplets traversing it [19].

2.2. Splat formation

Experimental set-ups were developed to determine the velocity v_p, surface temperature T_p and diameter d of a single particle prior to its impact and then its temperature and surface evolutions during flattening as well as the surface temperature evolution of the resulting splat during its cooling. The interested reader can find a presentation of these set-ups in [12-14].

Other techniques allow the collection of a few thousands of splats all over the spray cone on a controlled temperature substrate to determine their diameter and shape factor distributions [13].

At last, a detailed observation of the structure of the splats collected on smooth surfaces can be obtained by Atomic Force Microscopy making it possible to see the details of the columnar growth [20].

The main results are as follows :

2.2.1. On smooth surfaces

Experimental evidences [21] have shown that there is a substrate critical temperature T_c, below which the splats are extensively fingered while over which, they have almost a perfect disk shape as shown in fig. 4. For ZrO_2 it was found that this transition temperature is between 450 and 550 K.

This phenomenon seems to be almost independent of the particle impact velocity. For example Table 3 presents results obtained with - 45 + 22 µm particles which velocities range between 200 m/s along the jet axis to 110 m/s at the limit of the spray cone. The data of this table correspond to about 3000 splats processed by image analysis. On the hot substrate, the mean Shape Factor $\overline{SF}$ is close to one, both in the spray cone central part and its periphery even if the mean splat diameter D is slightly smaller in the spray cone periphery, as it could be expected. SF is defined as $4\,\Pi\,S/P^2$ where P is the splat perimeter and S its surface area ($SF = 1$ for a disk). For cold substrates D is by far smaller due to material splashing and $SF \sim 0.67$ against 0.94. The dispersion is also higher. However, if the substrate is oxidized (due to a too long preheating) splats are again extensively fingered. The oxidation stage depends strongly on the preheating time with the plasma jet and the substrate material [20,22]. Splat cooling rates, measured by fast pyrometry [12-14], are 3-6 times higher with the hot substrate. For the disk shape splats obtained at 573 K, the splat cooling theoretical curve [23] of a 1-D model has been adjusted to the experimental curve by varying the thermal contact resistance. Values of $R_{th} \sim 10^{-7}$ - 10^{-8} $m^2.K/W$ were obtained corresponding to an almost perfect contact as confirmed by the crack network due to quenching stress relaxation observed in fig. 4.b. On cold substrates, the contact resistance R_{th} calculated assuming that the splats have a disk-shape, were found to be of the order of 10^{-6} m^2K/W. This poor contact resistance is confirmed by the pulling off of splats by the tip of a perthometer. This does not occur when splats are collected on hot substrates.

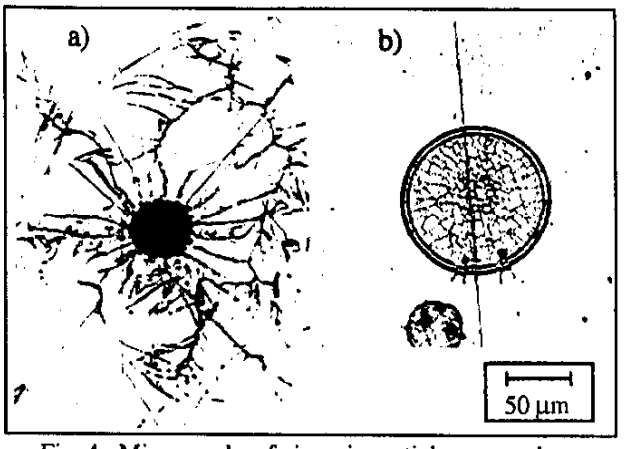

Fig. 4 : Micrographs of zirconia particles sprayed, on (a) 350 K substrate, (b) 550 K substrate (impact velocity ~ 200 m/s).

Substrate temperature T_{ph} (K)	350		573	
Analyzed area	center	periphery	center	periphery
D splat mean diameter (µm)	67 ± 24	59 ± 20	107 ± 44	101 ± 36
SF shape factor (µm)	0.68 ± 0.20	0.67 ± 0.21	0.95 ± 0.13	0.94 ± 0.12
CR cooling rates (K/µs)	100-200	--	500-800	--

Table 3 : Splat mean diameter D, shape factor SF and cooling rate CR with substrate temperature and location within the spray cone.

The latter exhibit on their whole surface, a homogeneous microstructure with a columnar growth perpendicular to the surface [20] (see fig. 5.a) except in the splat rim (see fig. 5.b) where the columnar structure is parallel to the substrate. Indeed, due to splat curling [24] the rim is not in contact with the hot substrate and cooling occurs through the already solidified columnar structure of the central part of the splat resulting in a columnar structure parallel to the substrate. As the cooling is much slower, the size of the columns is bigger. On cold substrates ($T_{ph} < T_c$) only a very few AFM measurements could be done, the splats being pulled off very easily. In this case, the central part of the splat consists of a few islands where the contact is good (columnar structure), however with bigger columns than on hot substrates, surrounded by rims where the crystal growth is parallel to the substrate [20]. The "fingers" exhibit the same morphology as that of the rims. As a general rule, the size of the columns depends very strongly on the cooling rate as illustrated in Table 4 for two different substrate materials and spraying equipments. With the RF plasma torch, the particle impact velocities are lower than 80 m/s resulting in splat thicknesses e_s in the range 2-2.5 µm against 0.9-1.2 µm with d.c. plasma torches. These thicker splats cool down slower (in a ratio 6-10) than the thinner splats.

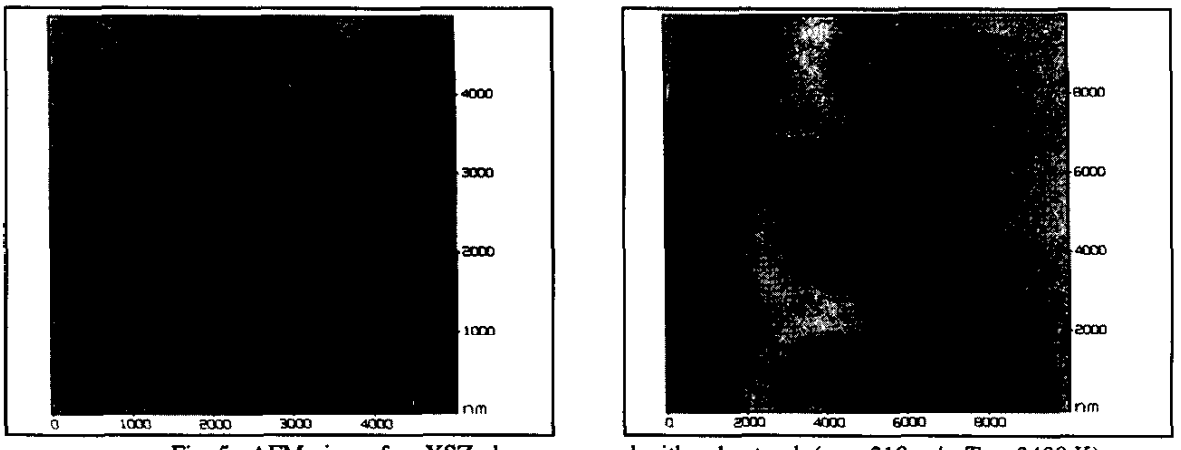

Fig. 5 : AFM view of an YSZ plasma sprayed with a d.c. torch (v_p = 210 m/s, T_p = 3400 K) (a) splat central part (note the cracks) (b) splat rim.

Plasma torch	d.c. torch with a 7 mm i.d. nozzle		r.f. torch with a 50 mm i.d.	
substrate material	stainless steel 304	YSZ	stainless steel 304L	YSZ
splat thickness e_s (μm)	0.95		2.2	
CR cooling rate (K/μs)	645	115	105	16
t_s solidification time (μs)	0.74	1.23	4.54	7.6
column width (nm)	125	250	320	>400

Table 4 : YSZ column width with respect to cooling conditions [19].

To explain the occurence of the critical temperature, Vardelle et al. [11,14] have proposed to compare the time t_{ft} at which flattening is almost completed (t_{ft} ~ 0.3-0.4 x t_f) to the time t_n corresponding to the onset of nucleation (see fig. 6). If $t_n > t_{ft}$, nucleation starts only when flattening is almost completed and it covers the whole splat surface allowing it to keep its disk shape. This is confirmed by the observation of splats collected on tilted substrates : these splats exhibit an elliptical shape with a larger thickness in the direction of the inclined substrate. If $t_n < t_{ft}$ nucleation starts at a few points which impede the liquid flow, resulting in splashing, which seems to be confirmed by the AFM splat study. t_n depends strongly on the maximum value of the interface temperature T_i which, in turn, is linked to the preheating temperature T_{ph}.

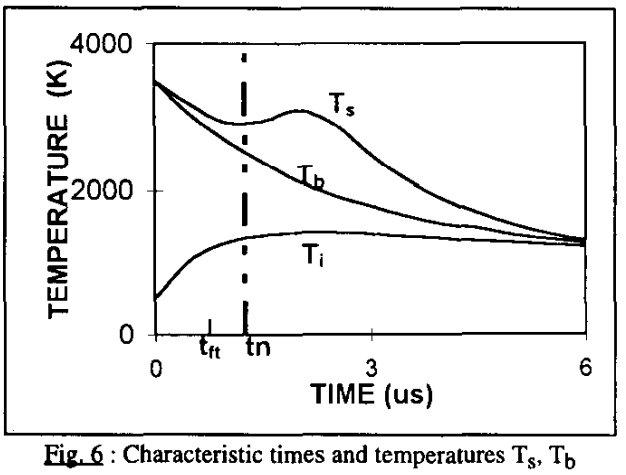

Fig. 6 : Characteristic times and temperatures T_s, T_b and T_i at splat surface, splat bottom and interface respectively ; T_{ph} is the substrate preheating temperature.

2.2.2. On rough surfaces

Fig. 7 shows SEM pictures (back scattered electrons) of zirconia splats collected on rough 304L substrate (Ra ~ 6 μm) [13]. It can be seen that, compared to smooth substrates, the particles are by far more extensively fingered but here again the contact is much better with the hot substrate as shown by the microcrack network exhibited by splat surface. The splats collected on rough substrates are thicker. This results in a drop of the splat cooling rate. On the 304L stainless steel substrates CR was found to be about 650 K/μs for smooth hot substrates and 120 K/μs for cold substrates With the rough substrates, the drop in CR is lower.

2.3. Coating formation

2.3.1. Thin passes

Coatings were sprayed [13,25] on a rotating substrate holder 110 mm in diameter in front of which

the torch was moved parallel to the holder axis. The substrates were either buttons (∅ = 25 mm, e = 6 mm) or beams (2 x 100 x 15 mm³) made of cast iron FT25 (only botton type), ordinary steel XC38, stainless steel 304L and Inconel 100.

The adhesion/cohesion (A/C) of coatings is closely linked to residual stresses [26,27]. Beside those resulting from grit blasting which play a role in A/C [28], the two most important are the quenching stress σ_q which is rather low for YSZ coatings [29] (σ_q < 20 MPa) and the expansion mismatch stress $\sigma_{\Delta\alpha}$ which depends strongly on the temperature difference between the constant spraying temperature T_d and room temperature. In order to reduce as much as possible residual stresses, YSZ coating thickness was limited to 300 µm and the pass thickness was 3 µm thanks to a fast relative movement torch/ substrate. In such conditions as measured σ_q ~ 8 MPa [25] and $\sigma_{\Delta\alpha}$ ~ -15 MPa at 300°C and -36 MPa at 500°C on 304L stainless steel. Thus the stress difference at the interface substrate coating is rather low and the coating adhesion/cohesion A/C, measured using the test DIN 50150 is mainly pure A/C. Table 5 presents typical A/C values obtained on 304L stainless steel, each result corresponding to the mean value of 5 measurements. It can be seen, that A/C values increase with substrate temperature but decrease with preheating time. This result is in good agreement with the previous observations on splat formation.

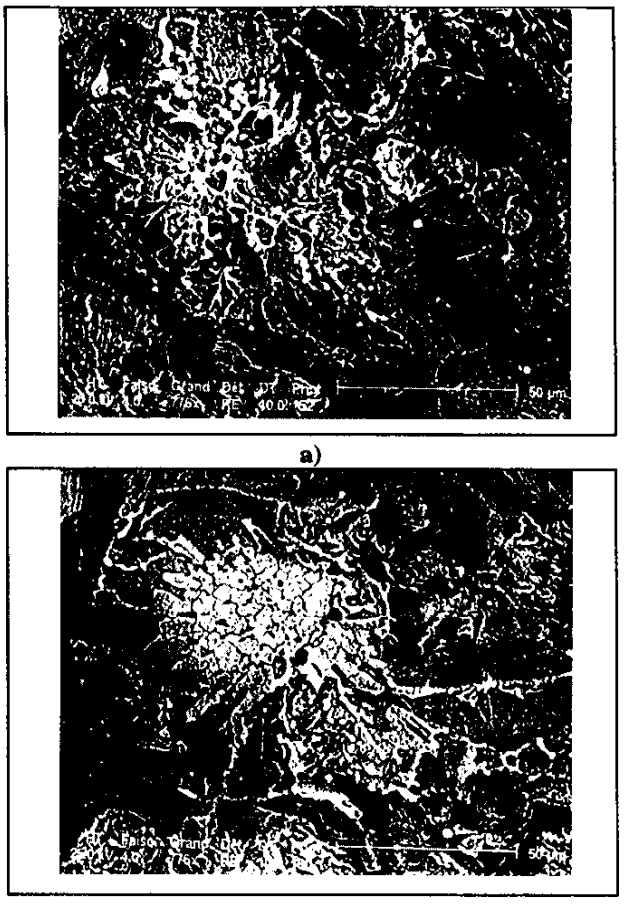

a)

b)

Fig. 7 : Splats collected on rough substrates (Ra ~ 5-6 µm). a) T_{sub} = 350 K, b) T_{sub} = 573 K.

Preheating temperature (K)	573 K				773 K			
Preheating time (s)	0	60	300	900	0	120	300	900
Coating adhesion/cohesion A/C (MPa)	20±2	50±2	40±2	31±4	20±2	64±5	49±2	45±2

Table 5 : Coating adhesion/cohesion (A/C) values on 304 stainless steel substrates preheated by the plasma jet at two different temperatures for different times.

The decreasing in A/C values when the preheating time increases is explained by the time-growth and time-composition change of the oxide layer at the 304L surface, as shown by recent studies [22] : the plasma plume contains atomic oxygen and oxidation is somewhat different from that obtained by preheating substrates in a furnace. Similar results are obtained on FT25, XC38 and In 100 substrates for different temperatures and preheating times. The coating Young's modulii obtained by comparing the deflections of XC38 beams measured during spraying [25,28] with values calculated using a 1-D code based on the equations proposed by Tsui and Clyne [30], are in the range 20-30 GPa. However, the precision is poor (± 30%) with such low values.

2.3.2. Thick passes

In order to limit oxidation problems 300 µm thick coatings sprayed on In 100 substrates were preheated to different temperatures and the pass thickness was varied from 25 to 300 µm/pass. With 25 µm passes for preheating temperature T_{ph} over 873 K, σ_q is more than doubled : 20 MPa against 8 MPa. For T_p ~ 973 K, the fractured cross section of coatings exhibits a columnar structure growing through the whole coating (see fig. 8.a). The Vickers hardness with a 5N load is increased to 1200 ± 80 MPa against 800 ± 70 MPa with the 3-µm thick pass (with T_p = 773 K). Unfortunately when spraying on In 100 substrates preheated at 973 K, the coating detached upon cooling probably due to oxidation problems.

a) b)

Fig. 8 : Fractured cross section of an YSZ coating :
a) at x = 0.4 mm from substrate and sprayed on an already deposited YSZ coating (300 μm on In 100) preheated at 973 K e_p = 25 μm, b) sprayed on In 100 preheated at 973 K, x = 0.005 mm.

When spraying on In 100 at 873 K with e_p = 80 μm, the first 25-30 μm exhibit no columnar growth except for 2-3 layered splats and afterwards a columnar growth through the whole coating. When measuring continuously the beam deflection, a slope change occurs after the time corresponding to the first 25-30 μm corresponding successively to σ_q = 8 and 22 MPa. The Young's modulus of this last part is 100-120 GPa against 50 GPa for the first 25-30 μm. During A/C tests, debonding takes place in the first 25 μm and the maximum A/C value reaches 40 MPa which could be explained by the tougher layer after 25 μm [27]. However, it must be underlined that with hot surfaces the sticking of the small (< 1 μm) droplets resulting from YSZ particles evaporation and recondensation [31] has to be carefully avoided between successive passes because it reduces the A/C values by a factor at least of 2. The columnar growth through layered splats and successive passes can be explained on the basis of the temperature diagram shown in Fig. 2. Calculations with thick passes (e_p > 25 μm) and T_p ~ 973 K show that nucleation of the impacting splat is delayed almost to the end of particle flattening ($t_n \sim t_f$) which could promote the columnar growth with the columns of the underlying solidified splat as nucleation sites.

3. REPRODUCIBILITY OF THE PLASMA SPRAY PROCESS

In industrial conditions the reproducibility of coatings is by far the most important problem and many parameters have to be controlled either before spraying or on-line during spraying, and assessed by coating analysis.

3.1. Powders

3.1.1. Characteristics

The main parameters are the YSZ particles chemistry and distribution of stabilizer within each particle, shape, density and size distribution. The first three parameters are closely linked to powder manufacturing process [32] and the last one to sieving. The density of the starting particles is one of the key parameter, the best results for coating thermomechanical properties being obtained with dense particles such as fused and crushed ones [33] or agglomerated and densified ones [34]. The stabilizer distribution within each particle has also a great influence which is enhanced by the faster evaporation of the Y_2O_3 stabilizer compared to ZrO_2. That is probably why particles made by sol-gel process, and then plasma densified, allow to increase the thermal shock resistance of the corresponding coatings by about 100°C compared to fused and crushed particles [35]. In the sol-gel technique Y_2O_3 grains, in the 0.1 μm size range, are uniformly distributed within each particle. Moreover, it has been shown that after plasma treatment, fused and crushed powders present a better homogeneity than agglomerated ones, sintered or not [36].

Another important questions is which particle size range has to be used : rather narrow such as - 45 + 22 μm or large - 106 + 10 μm ? and which lower limit 22, 10 or 5 μm ? The answers depend on the desired properties. As a general rule, YSZ particles which diameter is over 50-60 μm are not fully molten with d.c. plasma torches because of the heat propagation phenomenon in the particles [37]. Thus, powders with a large particle size range may result in coatings with higher porosity but lower mechanical

resistance. For the lower limit of the particle distribution the injection problems are critical. Most of small particles, especially those below 10 μm, hardly penetrate within the plasma jet, travel in its periphery and are sucked down farther downstream resulting in defects in the coating when they stick to it, which is especially the case when the coating surface is kept over 773 K during spraying.

3.1.2. Powder injection in the plasma-jet

Internal injection allows a better penetration of the particles within the plasma jet compared to external injection [37]. However with small particles, requesting a higher carrier gas flow rate, the plasma flow perturbation is more important with internal injection [38]. The position of the injection port and its distance z from the torch axis is very critical. A variation of z of a few tenths of mm modifies deeply the particles mean trajectory. Thus, any change in the injector port location and its wear have to be checked very carefully and regularly. It is also the case of the internal wear of the injector, a rough internal surface modifying deeply the powder distribution at the injector exit compared to that obtained with a new injector with a smooth internal surface. More precisely (see section 3.2.2) the trajectory distribution of particles within the plasma jet has to be followed continuously because it controls acceleration and heating of the particles.

3.2. Plasma spray process

3.2.1. Wear of the electrodes

The arc behavior at the anode and cathode is quite different. Thoriated tungsten cathode tip wear is rather fast (~ 1 h). It is due to the fast diffusion of thoria which increases drastically the cathode tip temperature (by about 1000 K) and induces a neck erosion below the tip which is blown up after a while [39,40]. The transition of a sharp cathode tip to a rounded one, which extremity becomes slowly and progressively wider, induces, within the first working hour, a reduction of the flow velocity of about 20% and a reduction of the arc voltage of 4 to 6% [41]. The widening of the cathode tip reduces progressively the voltage by 5-8% after 20 h, and the jet velocity by about 10%.

The arc root fluctuations (restrike mode) [41,42] which condition the arc root life time and thus the anode erosion, evolve with operation time and number of torch ignitions. This erosion is distributed in an area which length is about 1.5 x d (d being the internal diameter of the anode). The depth of the eroded area as well as the life time of the arc root increase with the operation time. Anode erosion results in an increase of the jet instability and a decrease in jet length coupled with a decrease in coating quality. When a tungsten insert is used this erosion problem may become even more critical when tungsten particles are ejected and imbedded within coatings. Therefore, it is important to monitor the anode erosion by the statistical analysis of the voltage signal [43] or its power spectrum [44], and determine when this wear will induce poor quality coating, long before its failure.

This type of monitoring makes it possible to check rapidly a defective gun assembly resulting for example in a poor electrode centering ; a non symmetrical arc attachment influencing deeply the restrike mode frequency and the voltage signal evolution.

3.2.2. Real time control

The outputs that have to be set and maintained are the particles mean temperature, velocity, trajectory and the substrate and then coating surface temperature before (preheating), during and after (cooling down) spraying. Among these parameters the most important, at least to our opinion, are the two last ones.

Substrate and coating temperature control depends strongly on the size, shape and thickness of the parts to be coated, the relative movements between the torch and the substrate and powder feed rate, linked to the pass thickness, and cooling means. If the surface temperature can be followed by IR pyrometry, the close-loop controller has to be designed according to substrate and coating heating and cooling, if possible by using simplified 1-D or 2-D computer codes easily adaptable to different geometries and pass thicknesses.

The mean trajectory of the particles within the plasma jet is very sensitive to the powder injection conditions which have to be adapted to the spraying conditions [37]. With a 1-D photodiode array, it is possible to follow continuously the hot particles distribution and, when coupling it to a laser sheet, to have simultaneously the trajectory distribution of the cold particles. The hot particles distribution is very sensitive to any variation of the injection parameters [46]. For example with ZrO_2 particles (- 45 + 22 μm) a variation of the powder feed rate of 50 g can be seen and the signal intensity is multiplied by 1.9 when the powder flow rate is doubled (from 1 kg/h to 2 kg/h). Only 1.9 and not 2 due to the starting of the load effect. Any change of the optimum carrier gas flow rate m°_{cg} modifying the trajectory is immediately detected. For example a change of 10% relatively to

its optimum value induces a 10% change of the signal amplitude and position.

Of course, it is also possible to control on line the surface temperature of the particles prior to their impact [47] or together the temperatures, velocities and trajectories of the particles [48]. These robust easy-to-use optical sensors, now commercialized, allow us, after positioning the torch in front of the sensor head for 1 minute, to check in industrial conditions the optimization of the spray parameters and their time evolution. For this last point after a certain spraying time the torch has to be positioned again in front of the sensor head. Such devices make them possible to determine when the load effect becomes important, measure the time necessary before reaching the stability of particle spraying conditions, increase the reproducibility of the spraying process.

Conclusion

Plasma sprayed TBCs thermomechanical properties depend strongly upon the contacts between splats and substrate and layered splats.

A better understanding of yttria partially stabilized (YSZ) splat formation made it possible to find a critical substrate preheating temperature T_c, in the 400-500 K range over which these contacts are strongly improved whatever may be the metallic substrate or the YSZ previously deposited layers. It seems that preheating over T_c increases the splat-substrate interface temperature allowing delay the time t_n at which nucleation starts to a value higher than the time to achieve an almost completed flattening. The adhesion/cohesion (A/C) of coatings increases with preheating temperature T_{ph} provided the substrate oxidation is limited. With 304 L stainless steel or In 100 substrates which oxidation resistance is good. A/C values can reach 70 MPa with T_{ph} = 773 K and a preheating time with the plasma torch below 120 s.

To compete with EB-PVD coatings, conditions have been searched to have a columnar structure through the whole coating (up to 1 mm thick). This structure is obtained when substrate or coating temperature reaches about 973 K. According to oxidation problems, when spraying in air, the substrate temperature has to be kept below this temperature and thus the first 20 μm of the coating do not exhibit this columnar structure but works are in progress to solve this problem. When spraying under such conditions the quenching stress increases drastically (from 8 to 25 MPa) with a corresponding increase of the coating Young's modulus (from 50 to 150 GPa). Therefore, to control the induced residual stresses, temperature of substrate and coating have to be monitored continuously by adjusting the pass thickness and the cooling devices to the coated part dimensions with the help of simplified 1-D or 2-D computer codes.

At last, to improve coatings reproducibility, strongly linked to the molten state and velocity of impacting particles, a rather simple set-up has been developed giving in real time the trajectory distribution of hot particles within the plasma jet and allowing to check any change in powder flow rate, carrier gas injection flow rate, injector wear... Compared to commercial set-ups following particle velocity, surface temperature and flux density it is by far much simpler and seems to be as efficient. The erosion of the torch nozzle has also to be followed by analyzing the voltage fluctuations which vary drastically when conditions are reached where coating quality is affected and allows also the detection of defective gun assembly.

Nomenclature

A/C	adhesion/cohesion (MPa)
APS	Atmospheric Plasma Spraying
CR	cooling rate (K/μs)
D	splat mean diameter (μm)
d	particle diameter (μm)
e_p	pass thickness (μm)
e_s	splat thickness (μm)
R_e	Reynold's number (dimensionless)
R_{th}	thermal contact resistance (m^2.K/W)
SF	splat shape factor (dimensionless)
T_b	temperature of the lower surface of the splat (K)
T_d	equilibrium temperature reached by coating upon spraying (K)
T_i	interfacial contact between splat and substrate (K)
T_m	particle melting temperature (K)
T_p	particle impact temperature (K)
T_{ph}	substrate preheating temperature (K)
t_f	flattening time (μs)
t_{ft}	time at which flattening is almost completed (μs)
t_j	time between two successive impacts (μs)
t_n	time at which nucleation starts (μs)
t_s	time at which solidification is completed (μs)
t_t	time between two successive passes (μs)
v_p	particle velocity at impact (m/s)
W_e	Weber's number (dimensionless)
μ_p	molten particle viscosity (kg/m.s)
ρ_p	particle specific mass (kg/m^3)
σ_p	molten particle surface tension (N/m)
ξ	flattening degree (ξ = D/d)

References

[1] W.J. Brindley, Journal of Thermal Spray Technology 5 (4) (1996) 379-380.

[2] W.A. Nelson and R.M. Orenstein, Journal of Thermal Spray Technology 6 (2) (1997) 176-180.

[3] W.P. Parks, E.E. Hoffman, W.Y. Lee and I.G. Wright, Journal of Thermal Spray Technology 6 (2) (1997) 187-198.

[4] D.W. Wortman, B.A. Nagaraj and E.L. Duderstadt, Mater. Sci. Eng. A121 (1989) 443-440.

[5] R.A. Miller, Surf. Coat. Technol. 30 (1987) 1-11.

[6] B.C. Wu and E. Chang, Thin Solid Films 172 (1989) 185-196.

[7] M. Yoshida, K. Abe, T. Aranami and Y. Harada, Journal of Thermal Spray Technology 5 (3) (1996) 259-268.

[8] S. Sodevka, M. Sazaki and K. Ueno, Journal of Thermal Spray Technology 5 (3) (1996) 277-282.

[9] D.V. Rigney, R. Vignie, D.J. Wortman and D.W. Skelly, Journal of Thermal Spray Technology 6 (2) (1997) 167-175.

[10] A. Maricocchi, A. Bartz and D. Wortman, Journal of Thermal Spray Technology 6 (2) (1997) 193-198.

[11] A. Vardelle, N.J. Themelis, B. Dussoubs, M. Vardelle and P. Fauchais, Transport and chemical rate phenomena in plasma sprays, J. of High Temp. Material Processes 4 (1997), to be published.

[12] P. Fauchais, M. Vardelle, A. Vardelle, L. Bianchi and A.C. Léger, Plasma Chemistry Plasma Processing 16 (1) (1996) 99S-126S.

[13] L. Bianchi, A.C. Léger, M. Vardelle, A. Vardelle and P. Fauchais, Plasma Sprayed zirconia splat formation and cooling, accepted in Thin Solid Films (1997).

[14] P. Fauchais, A.C. Léger, M. Vardelle and A. Vardelle, Formation of plasma-sprayed oxide coatings, in Proc. of J. Szekely Memorial Symp. on Materials Processing (Pub.) TMS (1997).

[15] M. Pasandideh-Fard, Y.M. Quiav, S. Chander and J. Mostaghimi, Physics of Fluids 8 (1996) 650-659.

[16] H. Fukanama, in Thermal Spray : Practical Solutions for Engineering Problems (ed.) C.C. Berndt and H. Herman, (Pub.) ASM Int. OH, USA (1996) 647-656.

[17] S. Kuroda, T. Dendo and S. Kitahara, Journal of Thermal Spray Technology, 4 (1) (1995) 75-84.

[18] F. Monerie-Moulin, F. Gitzhofer, P. Fauchais, M. Boulos and A. Vardelle, J. of High Temp. Chem. Processes 1 (3) (1992) 249-257.

[19] A. Haddadi, F. Nardou, A. Grimaud and P. Fauchais, in Advances in Thermal Spray Science and Technology (eds.) C.C. Berndt and S. Sampath (Pub.) ASM Int. OH, USA (1995) 249-254.

[20] L. Bianchi, A. Denoirjean, F. Blein and P. Fauchais, Thin Solid Films 299 (1997) 125-135.

[21] M. Fukumato, S. Katoh and I. Okane, Proc. of 14th ITSC (Ed.) A. Ohmori (Pub.) High Temp. Soc. of Japan, Osaka, Japan (1995) 353-358.

[22] A. Denoirjean, A. Grimaud, P. Fauchais, J. Pech and B. Hannoyer, Influence of substrate oxidation on alumina splats in plasma spraying, Proc. of United Thermal Spray Conf., Indiannapolis 15-18 Sept. (1997), (Pub.) ASM Int. OH, USA.

[23] A. Vardelle, M. Vardelle, P. Fauchais and D. Gobin, NATO Series E : Applied Science 282 (1995) 95-121.

[24] M. Bertagnoli, M. Marchese and G. Jaccuci, J. of Thermal Spray Technology 4 (1) (1995) 41-49.

[25] A.C. Léger, PhD Thesis (in French), Univ. of Limoges, France, March 12th (1997).

[26] T.W. Clyne and S.C. Gill, J. of Thermal Spray Technology 5 (4) (1996) 401-418.

[27] Y.C. Tsui and T.W. Clyne, see [16], (1996) 275-284.

[28] M. Mellali, P. Fauchais and A. Grimaud, Surf. and Coatings Technol. 81 (1996) 275-286.

[29] A.C. Léger, A. Grimaud, P. Fauchais and C. Catteau, see [16] (1996) 891-896.

[30] Y.C. Tsui and T.W. Clyne, An analytical model for predicting residual stresses in progressively deposited coatings. Part 1 : Plasma geometry, submitted to Thin Solid Films Dec. (1996).

[31] K.A. Gross, J. Tikkanen, J. Keskinen, P. Fauchais, M. Vardelle and A. Grimaud, Vaporization and ultrafine particle generation during the plasma spraying process, to be published in United Thermal Spray Conference, Indiannapolis Sept. (1997) (Pub.) ASM Int. OH, USA.

[32] H. Eschnauer, Thin Solid Films, 73 (1980) 1-17.

[33] F. Gitzhofer, A. Vardelle, M. Vardelle and P. Fauchais, Materials Science and Eng. A147 (1991) 107-120.

[34] A. Denoirjean, A. Vardelle, C. Martin, P. Fauchais, T. Cosack, E. Lugsheier, I. Rass, P. Chandler, R. McIntyre and H.L. Heijen, in Thermal Spray : Int. Advances in Coatings

Technology (Pub.) ASM Int. OH, USA, (1992) 967-982.

[35] D. Bernard, PhD's thesis, Univ. of Limoges, June 25 (1990).

[36] B. Kolman, J. Forman, J. Dubsky and P. Chraska, Mikrochim. Acta 114/115 (1994) 335-342.

[37] M. Vardelle, A. Vardelle and P. Fauchais, J. of Thermal Spray Technology 1 (2) (1992) 117-128.

[38] B. Dussoubs, A. Vardelle, M. Vardelle, P. Fauchais and N.J. Themelis, 13th Int. Symp. on Plasma Chem. 5 (1997) 2056-2061 (ed.) Prof. C.K. WU, Institute of Mechanics, Chinese Academy of Sciences, Beijing 100080, China.

[39] X. Zhou and J. Heberlein, Plasma Chem. Plasma Proc. 16 (1) (1996) 299S-244S.

[40] X. Zhou, B. Ding and J. Heberlein, IEEE Trans. Components Pkg. and Mfg. Tech. 19 (3) (1996) 320-328.

[41] P. Fauchais, J.F. Coudert and M. Vardelle, Transient phenomena in plasma torches and for plasma sprayed coating generation, accepted in J. de Physique III.

[42] J.F. Coudert, M.P. Planche and P. Fauchais, Plasma Chem. Plasma Proc. 16 (1) (1996) 211S-228S.

[43] M.P. Planche, PhD's thesis (in French), Univ. of Limoges, France (1995).

[44] Z. Duan, L. Beall, M.P. Planche, J. Heberlein and E. Pfender, Arc voltage fluctuations as an indication of spray torch anode condition, to be published in proc. of UTSC 97, (Pub.) ASM Int. OH, USA.

[45] K.I. Li, M. Vardelle and P. Fauchais, see [19] (1995) 59-66.

[46] M. Vardelle, A.C. Léger, A. Vardelle and P. Fauchais, Influence of the variation of plasma torch parameters on particle melting and solidification, to be published in Proc. of UTSC 97, (Pub.) ASM Int. OH, USA.

[47] W.D. Swank, J.R. Fincke and D.C. Haggard, see [19] (1995) 111-116.

[48] C. Moreau, P. Gougeon, A. Burgess and D. Ross, see [19] (1995) 141-147.